



# Modelling and analysis of nuclear reactor system coupled with a liquid metal battery

May 2024

*Changing the World's Energy Future*

Amey Shigrekar, Jiangkai Peng, Temitayo Olayemi Olowu, Fernando Gallego Dias, Tyler L Westover



#### **DISCLAIMER**

This information was prepared as an account of work sponsored by an agency of the U.S. Government. Neither the U.S. Government nor any agency thereof, nor any of their employees, makes any warranty, expressed or implied, or assumes any legal liability or responsibility for the accuracy, completeness, or usefulness, of any information, apparatus, product, or process disclosed, or represents that its use would not infringe privately owned rights. References herein to any specific commercial product, process, or service by trade name, trade mark, manufacturer, or otherwise, does not necessarily constitute or imply its endorsement, recommendation, or favoring by the U.S. Government or any agency thereof. The views and opinions of authors expressed herein do not necessarily state or reflect those of the U.S. Government or any agency thereof.

# **Modelling and analysis of nuclear reactor system coupled with a liquid metal battery**

**Amey Shigrekar, Jiangkai Peng, Temitayo Olayemi Olowu, Fernando Gallego  
Dias, Tyler L Westover**

**May 2024**


**Idaho National Laboratory  
Idaho Falls, Idaho 83415**

**<http://www.inl.gov>**

**Prepared for the  
U.S. Department of Energy  
Under DOE Idaho Operations Office  
Contract DE-AC07-05ID14517**

## ORIGINAL RESEARCH

# Modelling and analysis of nuclear reactor system coupled with a liquid metal battery

Amey Shigrekar<sup>1</sup> | Jiangkai Peng<sup>2</sup> | Temitayo O. Olowu<sup>1</sup>  | Fernando Gallego Dias<sup>3</sup> | Tyler Westover<sup>1</sup>

<sup>1</sup>Idaho National Laboratory, Idaho Falls, Idaho, USA

<sup>2</sup>National Renewable Energy Laboratory, Golden, Colorado, USA

<sup>3</sup>Midcontinent Independent System Operator, Inc., Carmel, Indiana, USA

## Correspondence

Temitayo O. Olowu, Idaho National Laboratory, Idaho Falls, Idaho 83415, USA.

Email: [temitayo.olowu@inl.gov](mailto:temitayo.olowu@inl.gov)

## Funding information

INL Laboratory Directed Research and Development (LDRD) Program, Grant/Award Number: DE-AC07-05ID14517

## Abstract

Traditionally, nuclear power plants in the U.S. provide baseload power to the power grid because they have less flexibility for ramping their output power than natural gas peaking plants. However, achieving climate goals to reduce the consumption of fossil-based natural gas places pressure on nuclear power plants and other power generators to ramp up their power output to balance grid generation with demand. This paper presents the modelling and performance analysis of a nuclear reactor system (NRS) coupled to a liquid-metal battery (LMB) to improve its dynamic response and enable its black start capability. The NRS and LMB thermal behaviour are modelled in Dymola, while the electrical dynamics of the LMB and power grid are modelled in RTDS-RSCAD. Both simulation platforms are coupled and share their thermal and electrical data using a Transmission Control Protocol/Internet Protocol (TCP/IP) communication protocol. The dynamic performance of the NRS-LMB integration is tested on the IEEE 9 bus, which demonstrates its ability to respond and provide frequency and voltage regulation. The black start capability of the NRS-LMB is also evaluated by simulating a grid outage and using the LMB to supply the auxiliary loads required to bring the NRS back online as soon as possible. The results show that coupling an NRS to an LMB improves the system dynamic performance and enables it to black start after being disconnected from the grid for several days.

## 1 | INTRODUCTION

To meet carbon emission goals, researchers are studying new ways of integrating clean energy systems to maximize efficiency and improve system flexibility. Recent large-scale implementations of solar and wind farms have rejuvenated the interest in renewable energy, driving down the costs of low-carbon electricity and utilizing domestically sourced alternatives to imported fossil fuels [1, 2]. Nevertheless, the intermittent nature of renewable energy is a source of instability in the grid and price fluctuations in the electricity market. For example, the capacity factor of wind and solar energies are less than 35 and 25%, respectively. Many options are being explored to provide flexibility to grid power systems, such as deploying dispatchable loads and utilizing electric vehicles as additional grid storage. A previous work showed that dispatchable clean hydrogen production can improve grid resilience [3]. Nuclear power is also

a promising option, considering that it provides stable power with a capacity factor typically over 92% [4]. However, nuclear reactor systems (NRSs) are not usually able to make large, rapid adjustments to the power they provide to the grid to help balance power generation and demand. A promising solution is to couple NRSs to dynamic energy storage systems, so that the integrated system can rapidly dispatch power to the grid and store excess energy during low demand periods [5]. By integrating NRSs with energy storage systems, it is possible to respond to grid dynamics reliably and effectively by storing and releasing energy as needed during peaks and troughs as a buffer between generation and demand. This approach allows nuclear reactors to operate stably near their rated capacities where they are the most profitable while also participating in energy arbitrage for improved economics. Energy storage may also enable integrated NRSs to participate in multicommodity markets [6]. Additionally, the integration of energy storage systems with NRSs could

This is an open access article under the terms of the [Creative Commons Attribution-NonCommercial-NoDerivs](https://creativecommons.org/licenses/by-nc-nd/4.0/) License, which permits use and distribution in any medium, provided the original work is properly cited, the use is non-commercial and no modifications or adaptations are made.

© 2024 The Authors. *The Journal of Engineering* published by John Wiley & Sons Ltd on behalf of The Institution of Engineering and Technology.

potentially ensure the availability of electrical power supply for its safety systems during safe shutdown or upon undesired events. Adequate power supply would fulfil the need for removing the decay heat, which is one of the main issues of nuclear reactor safety in the case of reactor shutdown [7]. According to [8], nuclear power plants can also be optimally located to ensure its internal loads can be powered from an off-site power system to ensure the continuity of power supply to the reactor power plant. This is necessary after any trip in order to prevent the reactor core from melting.

For this analysis, we selected a high-temperature gas reactor (HTGR) coupled to a supercritical CO<sub>2</sub> (sCO<sub>2</sub>) Brayton power cycle as the NRS due to the HTGR's high operating temperature, which can provide high-quality heat for a range of industrial processes, such as hydrogen production, desalination, synthetic fuel production, district heating etc. HTGRs also have key safety features, including their use of inert helium as the heat transfer fluid and inherent safety in the event that reactor coolant is lost [9, 10]. We chose the sCO<sub>2</sub> Brayton cycle for the power cycle due to its potential to yield high thermal efficiencies at lower capital costs than steam-based power cycles. Maintaining the working fluid near its critical point results in higher densities, which reduces the size of equipment and also the input power needed during the compression step [11, 12].

The energy storage system chosen for this analysis is a liquid-metal battery (LMB). This technology deploys two metal alloys, separated by a molten-salt electrolyte, resulting in an electrochemical reaction that allows electricity to be stored and discharged. LMBs can provide a large amount of current flow for fast frequency and voltage response and have a long duration storage capability suitable for reserve electricity markets. Unlike lithium-ion batteries, LMBs are not as sensitive to temperature variations. They do not explode or exhibit thermal runaway leading to uncontrolled combustion. They can withstand overcharging, overdischarging, and sudden short circuiting with a very low risk to safety. Because their electrodes and electrolytes are in molten state, LMBs have very fast diffusion and reaction kinetics, making them attractive for applications that require fast charging and discharging [13]. The liquid state of LMBs provides them with a self-healing capability so that they can potentially operate for long time periods with very low or no degradation [14].

Further benefits of LMBs are that they are made of environmentally friendly and abundant materials, such as calcium, magnesium, and antimony, and the manufacturing process is relatively simple [15–17]. According to one commercial manufacturer [18], LMBs are projected to cost 30–50% less than lithium-ion systems of the same size and configuration. A key factor in the lower cost of LMBs is their ability to operate in hot environments with very little auxiliary electricity. These features, along with their potential high efficiency [19] and flexible scalability [20], make them attractive for grid-scale applications.

In this work, dynamic integrated models are used to explore coupling an LMB to an NRS for improved dynamic performance of the integrated system. The main contributions are:

- Development of physics-based dynamic models for an NRS (HTGR and sCO<sub>2</sub> Brayton cycle) and an LMB. The designs for all components are based on published literature such that they are robust, scalable, and reproducible.
- Integration of HTGR, sCO<sub>2</sub> Brayton cycle, and LMB models as a combined power plant through co-simulation. The coupling of these models allows for accurate dynamic thermal and electrical analysis of the entire system.
- Analyses of case studies with a coupled NRS-LMB system for grid services and black start capability. The results show the ability of the NRS-LMB system to provide fast frequency and voltage regulation as well as the black start capability for remote or challenging applications in which grid power may not always be available.

In this paper, Section 2 presents the system overview and proposed approach, Section 3 presents the model development of the NRS and LMB, Section 4 describes the integration of the models using two different simulation platforms, Section 5 presents an analysis of the model performance, and Section 6 describes our conclusions and potential for future work.

## 2 | SYSTEM OVERVIEW AND PROPOSED APPROACH

Dynamic models of an HTGR, an sCO<sub>2</sub> Brayton cycle, and the thermal components of the LMB were developed in Dymola. All of these system-level models were developed as standalone models for ease of design and were connected to each other using ports. The HTGR model was based on Japan Atomic Energy Research Institute's HTGR-gas turbine (GT) concept, and model details can be found in [21]. This model was chosen because its operating conditions are readily available compared to other high-temperature reactors. However, the model was scaled down to an output of 20 MWt to simulate a microreactor. The decisions to analyze the system at a scaled level were due to the opportunities microreactors are expected to provide in the near future. These include faster, cheaper, and more efficient production of reactor modules, scalability, safer operation, and rapid deployment as an emergency response to help restore power in areas affected by natural disasters. The sCO<sub>2</sub> Brayton cycle model was based on a generic recompression system, the details of which were acquired from [22]. The power cycle was scaled down equivalently to couple with the reactor model. The scaled mechanical power from the sCO<sub>2</sub> turbine in Dymola is provided to a synchronous generator in RTDS that converts mechanical power to electricity. The LMB model was developed in two parts. One part analyzed the thermal aspect and was modelled in Dymola, while the other analyzed the electrical aspect and was modelled in Simulink and RSCAD. The electrical model of the LMB is coupled to the Dymola-based turbine output through a transformer, transmission lines, and converters. The overall LMB capacity was set to be 20 MWhe. A schematic of the proposed integration between the HTGR, sCO<sub>2</sub> power cycle, LMB, and grid is shown in Figure 1.

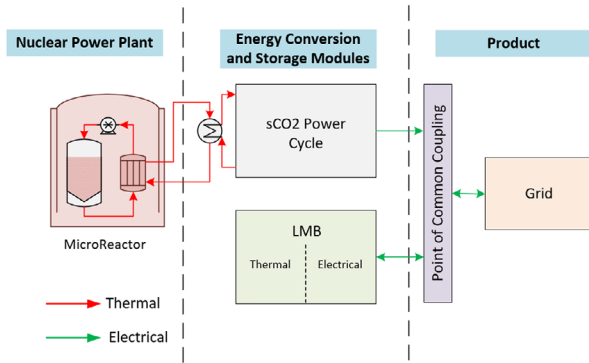


**FIGURE 1** Schematic of the proposed integration of HTGR, sCO<sub>2</sub> power cycle, and LMB.

The red connecting lines indicate thermal energy flow while the green connecting lines indicate electrical energy flow. As shown in Figure 1, heat from the microreactor is transferred to the sCO<sub>2</sub> power cycle via a secondary loop that contains a gas–gas heat exchanger. The coolant within the primary and secondary loops of the microreactor are helium, whereas that within the power cycle is sCO<sub>2</sub>. It is possible to transfer heat from the cooler of the power cycle to the LMB if needed during initial heat up phases, but that has not been analyzed herein. The electricity produced by the power cycle's generator is then sent to a point of common coupling, from where it could either be sent to the grid or the LMB. The following section describes the model development that was carried out for this analysis.

### 3 | MODEL DEVELOPMENT

We used two simulation environments (Dymola and RSCAD) to develop the submodels for this work. Dymola is a commercial modelling platform that allows the simulation of large and complex systems using mathematical equations to describe the dynamic behaviour of the components and interactions [23]. Several opensource libraries have prebuilt component-level models that can be used to develop a system-level model. The Dymola simulation platform modelled the NRS as well as the thermal aspect of the LMB. RSCAD is a simulation platform that can be used for the real-time, hardware-in-the-loop simulation of power system components, networks, and their controls [24]. The RTDS-RSCAD platform modelled the electrical aspect of the LMB, synchronous generator (for the NRS), and the Institute of Electrical and Electronics Engineers (IEEE) test system used in this study. This study leverages the strengths of both of these modelling platforms and uses a TCP/IP communication protocol to exchange the necessary data between them. The following section describes the individual models within the simulation platforms.

#### 3.1 | HTGR modelling

The HTGR system is a helium-based closed-loop cycle, in which the primary coolant flows through the reactor core,

**TABLE 1** Operating conditions of prototype and scaled HTGR-sCO<sub>2</sub> coupled systems.

Parameter	Prototype value	Scaled value
$P_c$	600	20
$\dot{m}_c$	296	9.87
$T_{i/o}^c$	450/850	450/850
$p_c$	60	60
$\dot{m}_t$	2,867	98.9
$T_{i/o}^t$	750/638	750/638
$p_t$	2.31	2.31
$P_n$	288	9.6
$\eta_s$	48	48

absorbing the heat, which is then transferred to the sCO<sub>2</sub> working fluid used in the power cycle. This heat transfer occurs via an intermediate heat exchanger with helium on the primary side and sCO<sub>2</sub> on the secondary side. Figure 2 shows the Dymola-based submodel of the HTGR cycle. The model uses standard Modelica-based components from the nuclear hybrid energy system (NHES) and transient simulation framework of reconfigurable models (TRANSFORM) packages available in Idaho National Laboratory's HYBRID repository [25] and the fluid package CoolProp [26] to model the sCO<sub>2</sub> fluid properties. The details of the core model can be found in [27].

The original HTGR-GT design has a thermal output of 600 MW, core mass flow rate of 296 kg/s, operating pressure of ~60 bar, and core inlet and outlet temperatures of 460 and 850 °C, respectively. As mentioned previously, the reactor was scaled down to 20 MWt to simulate a microreactor, and the scaled operating conditions of such a design are provided in Table 1. The geometric specifications and initialization parameters for the model are provided using the data blocks. The control mechanism implemented for this model on the primary loop aims to govern the reactor outlet temperature as well as the core power based on the mass flow rate through the core and its reactivity. A cooler has also been incorporated in the model to negate the heat generation due to the blower. The primary heat exchanger is a simplified component that uses the number of transfer units (NTU) method to calculate heat transfer between helium on the primary side and sCO<sub>2</sub> on the secondary side. The fluid ports port\_a and port\_b are the inlet and outlet fluid flow ports, respectively, and are used to connect the HTGR and sCO<sub>2</sub> power cycle submodels. The detailed description of the power cycle is provided in the next section.

#### 3.2 | sCO<sub>2</sub> power cycle modelling

The power cycle is a recompression sCO<sub>2</sub> Brayton cycle with an inter-cooler and a single stage turbine, with high- and low-temperature recuperators. Figure 3 shows the Dymola-based model of the power cycle used in this analysis, which was developed using components from the NHES and TRANSFORM packages.





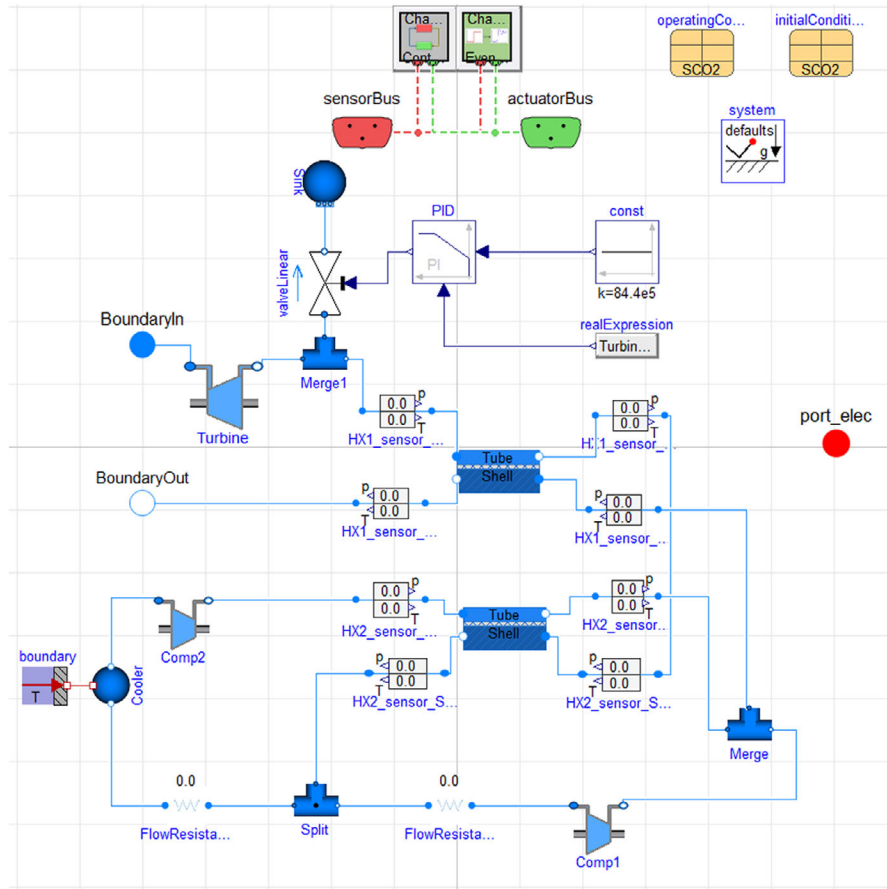


FIGURE 3 Dymola-based model of a simplified sCO<sub>2</sub> Brayton power cycle.

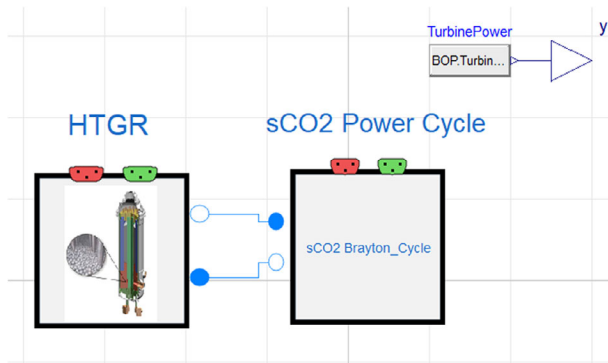


FIGURE 4 Dymola-based model of HTGR coupled to an sCO<sub>2</sub> power cycle.

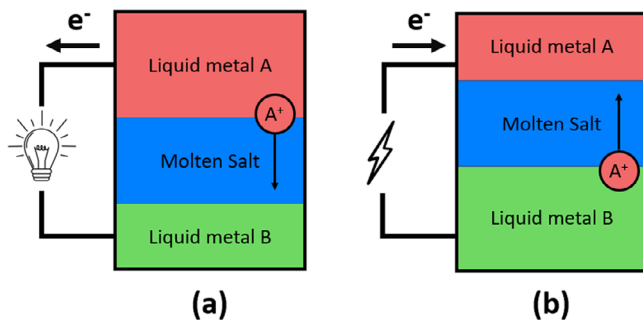


FIGURE 5 Schematic of an LMB discharging (a) and charging (b).

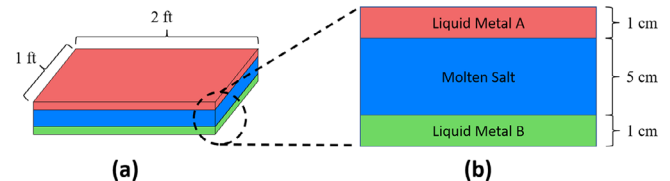


FIGURE 6 Isometric (a) and cross-sectional (b) views of an LMB with dimensions used in this analysis.

blocks are used to meet the need of 20 MWh. The approximate dimensions of a single LMB cell we used in this analysis are shown in Figure 6.

The electrical and thermal models that capture the electrodynamic and thermodynamic responses of the LMB, respectively, are described below.

### 3.3.1 | LMB thermal modelling

The thermal model assumes that 100 individual cells form an energy block nearly isothermal due to the high thermal conductivity of the liquid and solid materials. A lumped-capacitance model with a mass-averaged specific heat capacity is used for the energy block. To calculate the mass-averaged specific heat of the LMB, the specific heats of the individual components,



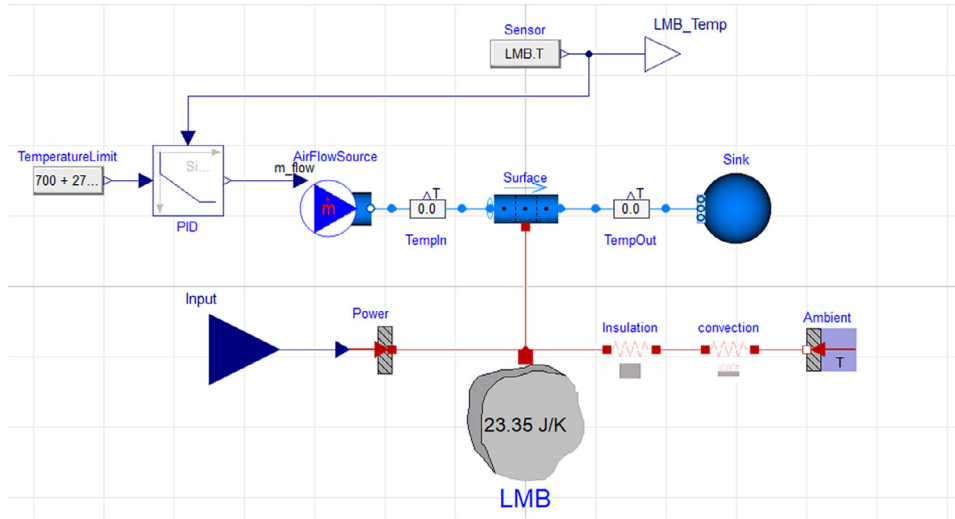


FIGURE 7 Dymola-based thermal model of a LMB.

namely, the two terminal electrodes and electrolyte at 700 °C, were multiplied with their respective mass fractions. The sum of these values provided the mass-averaged specific heat, which was then multiplied by the total mass of the LMB to calculate its capacitance. Insulation around the LMB energy block and its heat loss to the environment were modelled using thermal resistances, with the ambient temperature being provided as a boundary condition. The thermal insulation we used in this analysis was a 5-inch-thick ceramic fibre board, which has a thermal conductivity of 0.15 W/mK. The ambient air's temperature was assumed to be 25 °C and its convective heat transfer coefficient to be 25 W/m<sup>2</sup>K.

The thermal model includes a volumetric heat source that is calculated based on Joule heating calculated by the electrical model based on charging and discharging currents and material electrical resistivities. Figure 7 shows a representation of a lumped-capacitance thermal LMB model. The input port receives the Joule heating input signal from the electrical model. It should be noted that convection-generated flow within the liquid electrodes and electrolytes as described by [29] increases the effective thermal conductivities of the liquids, and consequently increases the effective Biot number, which further validates the assumed lumped thermal capacitance model used for the LMB energy block.

Additionally, a temperature control mechanism has been implemented to ensure the LMB temperature does not exceed 700 °C due to excessive Joule heating while charging or discharging. Cooling is achieved by blowing ambient air over the cells with flow control provided by a thermal management system. Battery cooling is simulated in Dymola by blowing air through a pipe with the same surface area and surface temperature as those of the LMB's energy block. The energy block surface area of 7.89 m<sup>2</sup> calculated by stacking 25 cells in four columns to attain 100 cells per block. A PID controller ensures the flow rate of air at 20 °C is controlled appropriately to meet the LMB maximum temperature set-point of 700 °C. Results of a representative LMB load test

are shown in Figure 8. The first plot, Figure 8(a), shows the power profile, which is varied between 10 and 12 kW, and Figures 8(b) and 8(c) show the corresponding LMB temperature and the cooling mass flow rate required to maintain the temperature.

### 3.3.2 | LMB electrical modelling

The electrical model of a LMB cell is derived from electrochemical fundamentals. It describes the relationship between the cell voltage  $E_{\text{cell}}$ , operating current density  $j$ , charge  $q$ , and temperature  $T$ . The dynamic operating voltage  $E_{\text{cell}}$  of an LMB cell can be represented as the equilibrium cell potential  $E_{\text{eq}}$ , accounting for active overpotentials  $\eta_{\text{mt}}$ ,  $\eta_{\Omega}$ , and  $\eta_{\text{ct}}$  [28].

The equilibrium cell potential  $E_{\text{eq}}$  is a function of the stage of charge  $q$ , LMB cell temperature  $T$ , while the mass transport overpotential ( $\eta_{\text{mt}}$ ), charge transfer overpotential ( $\eta_{\text{ct}}$ ), solution resistance overpotential ( $\eta_{\Omega}$ ) are functions of the stage of charge  $q$ , LMB cell temperature  $T$  and the cell exchange current density. The value of  $E_{\text{cell}}$  is as expressed in Equation (1)

$$E_{\text{cell}}(q, j, T) = E_{\text{eq}}(q, T) + \eta_{\Omega}(q, j, T) + \eta_{\text{mt}}(q, j, T) \cdot \frac{1}{1 + s\tau_{\text{mt}}} + \eta_{\text{ct}}(q, j, T) \cdot \frac{1}{1 + s\tau_{\text{ct}}} \quad (1)$$

where

$$q = \int j dt$$

In Equation (1)  $\eta_{\text{mt}}$  is the mass transport overpotential that arises from concentration gradients in the electrodes and electrolytes;  $\eta_{\text{ct}}$  is the charge transfer overpotential, resulting from the potential energy barrier to the interfacial reaction;  $\eta_{\Omega}$  is

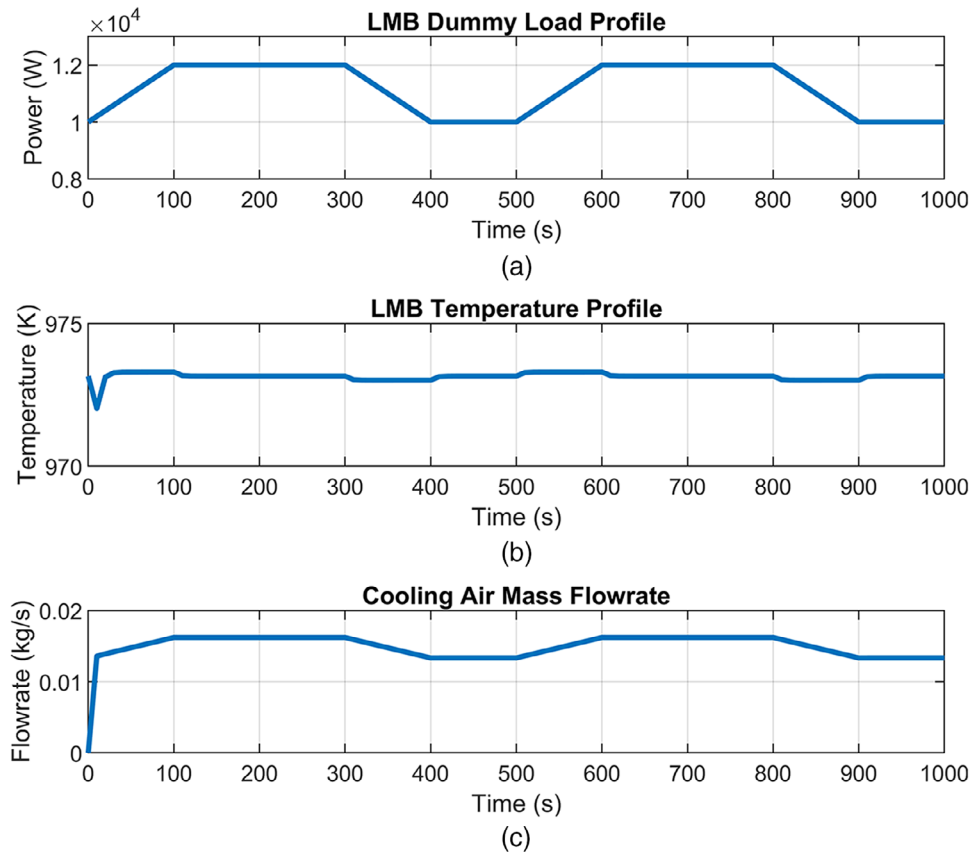


FIGURE 8 LMB temperature control mechanism test profiles.

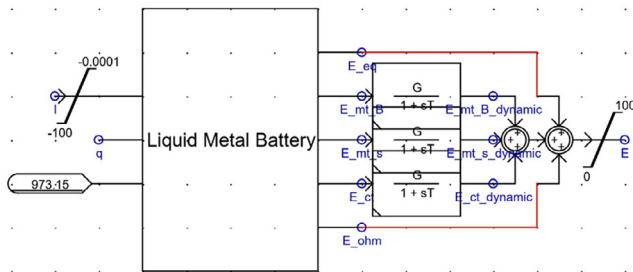


FIGURE 9 Schematic of RSCAD-based electrical model of the LMB.

the solution resistance overpotential due to irreversible resistive heat generation in the electrolyte; and  $\tau_{mt}$  and  $\tau_{ct}$  are first-order time constants associated with the cell's mass transfer and charge transfer dynamics, respectively. For this work we select the values of  $\tau_{mt}$  and  $\tau_{ct}$  as 0.1 s.

To facilitate model integration and real-time grid simulation, the LMB model is developed in the RSCAD simulation environment. The cell geometry and material property values of the electrical LMB model are based on experimental data obtained from a magnesium-antimony LMB [28]. Figure 9 shows a schematic of the RSCAD-based model.

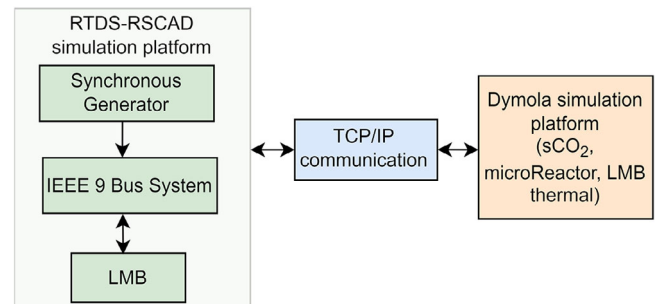


FIGURE 10 Schematic of the co-simulation of HTGR, sCO<sub>2</sub> power cycle, and LMB models.

## 4 | MODEL INTEGRATION

The LMB's voltage and power are scaled up by modelling the aggregation of multiple cells in series and parallel to achieve the desired open circuit DC voltage and power rating, which are 1.6 kV DC and 20 MWe, respectively. The scaled-up LMB model is connected to a three-phase inverter with grid-forming and grid-following controls. The AC voltage is filtered to remove the high-order harmonic contents of the inverter, and the AC output of the LMB's inverter is connected to a step-up transformer to achieve the desired bus voltage for connection to the NRS. As mentioned previously, the Dymola-based NRS model provides an output signal for the generated mechanical power, which is

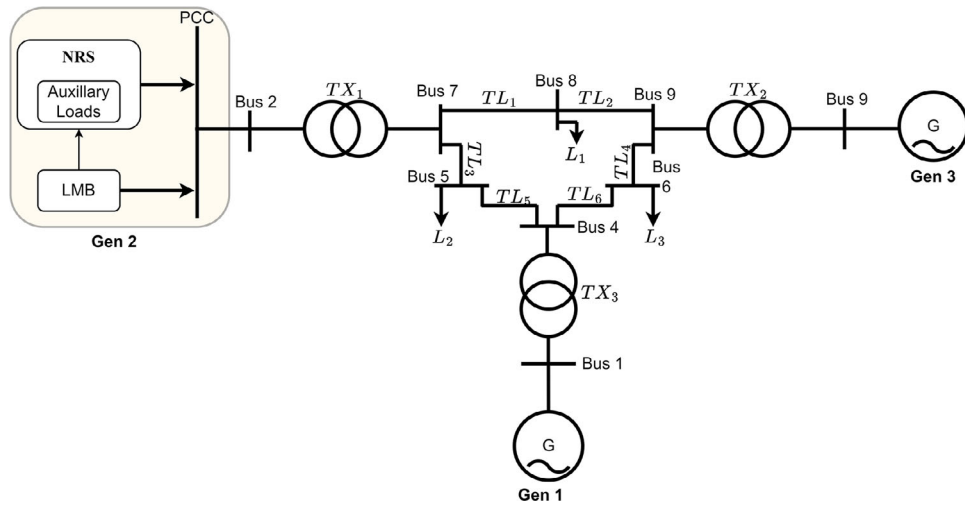


FIGURE 11 IEEE 9 bus system with NRS-LMB system at bus 2.

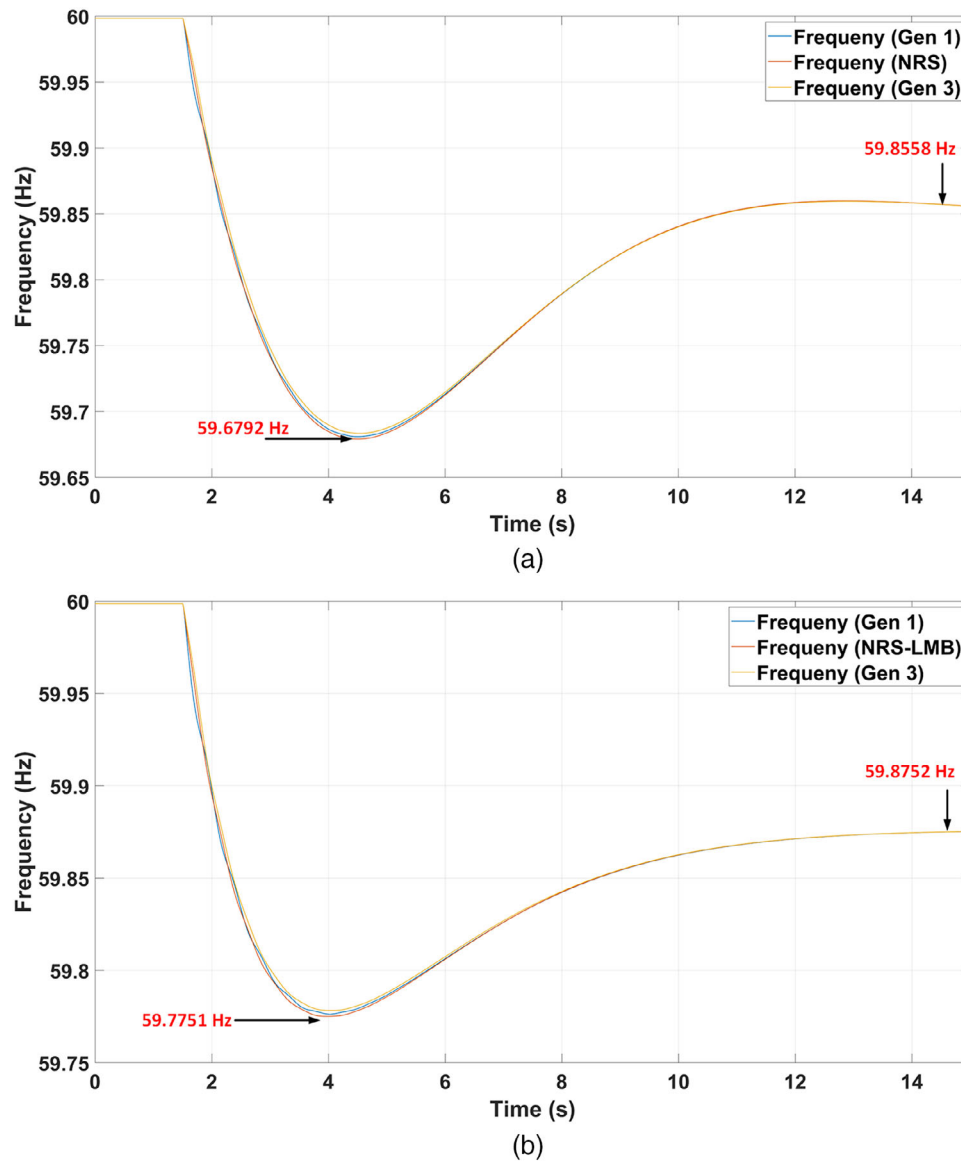


FIGURE 12 The generators frequency response before LMB integration (a) and after LMB integration (b).

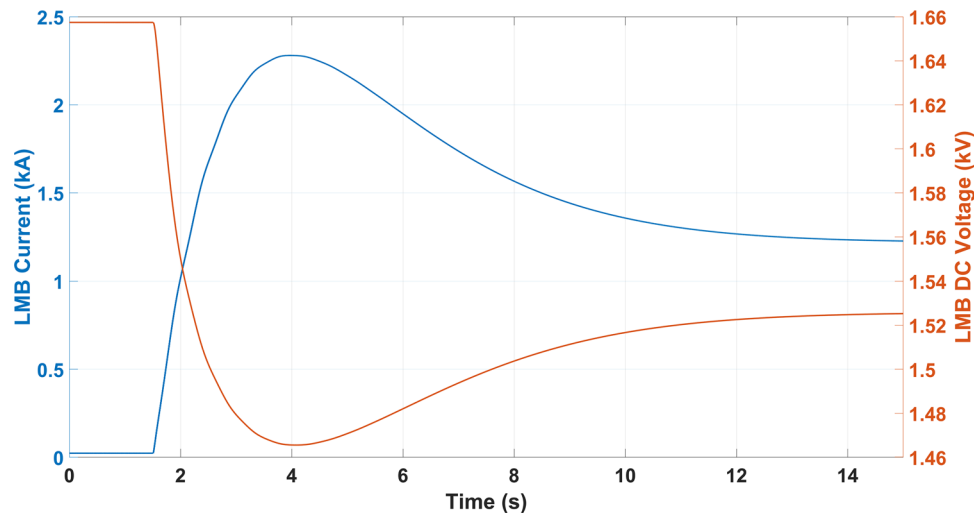


FIGURE 13 LMB DC voltage and current dynamic response.

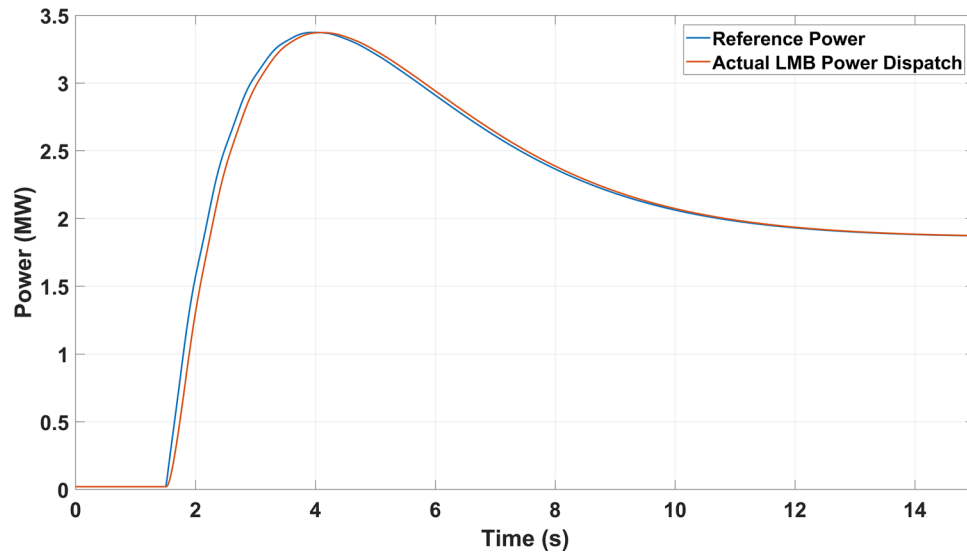


FIGURE 14 LMB Reference active power reference (based on frequency–Watt droop) and actual active power dispatch.

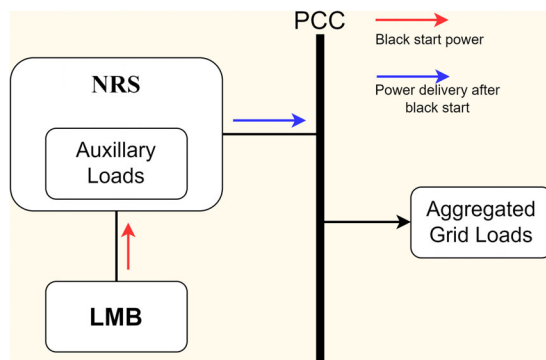


FIGURE 15 Schematic of a simulated black start architecture.

sent to RSCAD and connected to the synchronous machine model through its governor–turbine interface. The schematic

of the simulation setup is shown in Figure 10. A TCP/IP protocol is used to set up the communication between the Dymola and RTDS-RSCAD simulation environment. The LMB temperature is simulated using the thermal model of the LMB in the Dymola simulation environment. The LMB current data is transferred from the RTDS-RSCAD through the TCP/IP in order to estimate the LMB's temperature (including effects of Joule heating) using the Dymola model. The LMB's temperature is subsequently sent back to the RTDS-RSCAD LMB model.

## 5 | MODEL PERFORMANCE ANALYSIS

As described earlier, the NRS (combined HTGR and sCO<sub>2</sub> systems) and LMB thermal behaviour are modelled using Dymola, while the LMB, NRS synchronous machine, and the transmission grid (IEEE 9-bus) are modelled using RTDS-RSCAD.

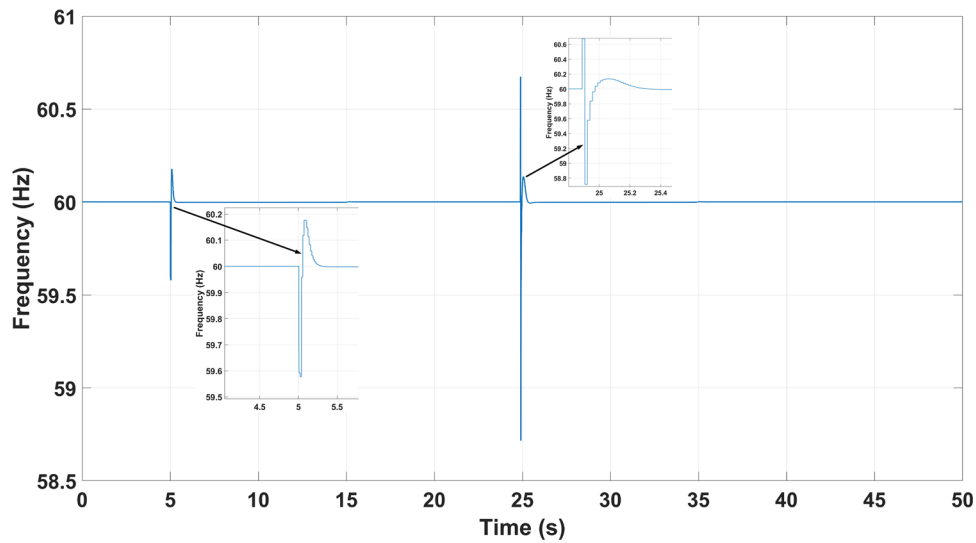


FIGURE 16 Frequency response during the black start scenario.

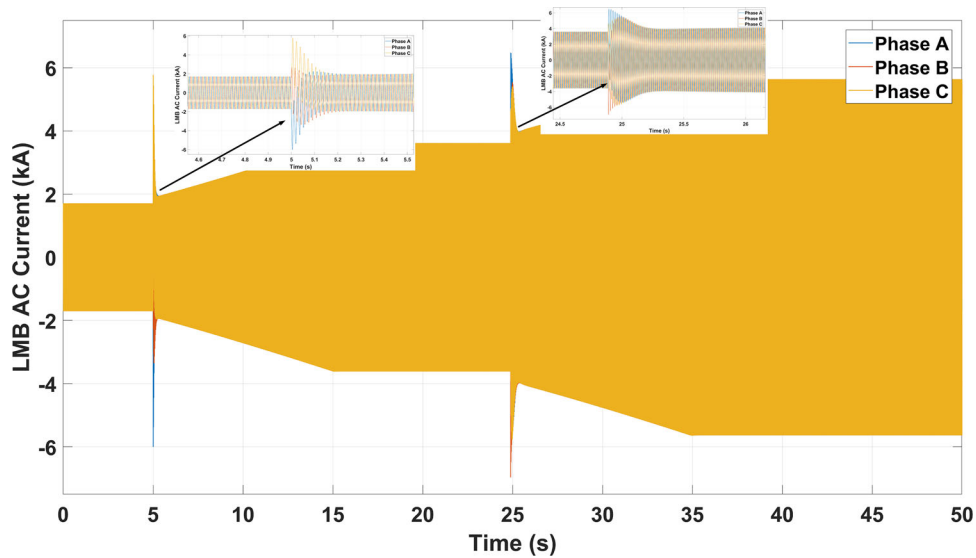


FIGURE 17 AC current dispatch by the LMB.

The dynamic performance of the modelled NRS-LMB system is investigated under two different test cases. The first test case involves using the coupled system to provide grid support while the second test case involves analyzing the ability of the NRS-LMB to provide a black start capability in the event of a grid failure.

### 5.1 | Grid-following performance analysis

In order to analyze the grid following performance of the coupled NRS-LMB, the system is integrated on with an IEEE 9 bus feeder. The IEEE 9 bus system consists of three P-Q loads ( $L_1$ ,  $L_2$ ,  $L_3$ ), six transmission lines ( $TL_1$ – $TL_6$ ), three transformers ( $TX_1$ – $TX_3$ ) and three generators (Gen 1, Gen 2, and Gen 3).

The generator located at bus two (Gen 2) is replaced with the NRS-LMB coupled system, as shown in Figure 11.

Two scenarios are modelled to validate the performance of the NRS-LMB system to provide grid-following services. In both scenarios, the load  $L_1$  connected to bus 8 is changed from 10 to 20 MW after the system achieves steady state. In the first scenario, the simulation includes only the NRS (without the LMB), while in the second scenario both the NRS and the LMB are included in the simulation. The simulation results showing the frequency nadir and the steady state frequency during the instantaneous change in Load  $L_1$  is shown in Figure 12.

The results show that, without the use of the LMB (with only the NRS), the frequency nadir during this change in load is 59.68 Hz and the final steady state frequency is 59.86 Hz. By coupling the LMB with the NRS, the frequency nadir is improved to

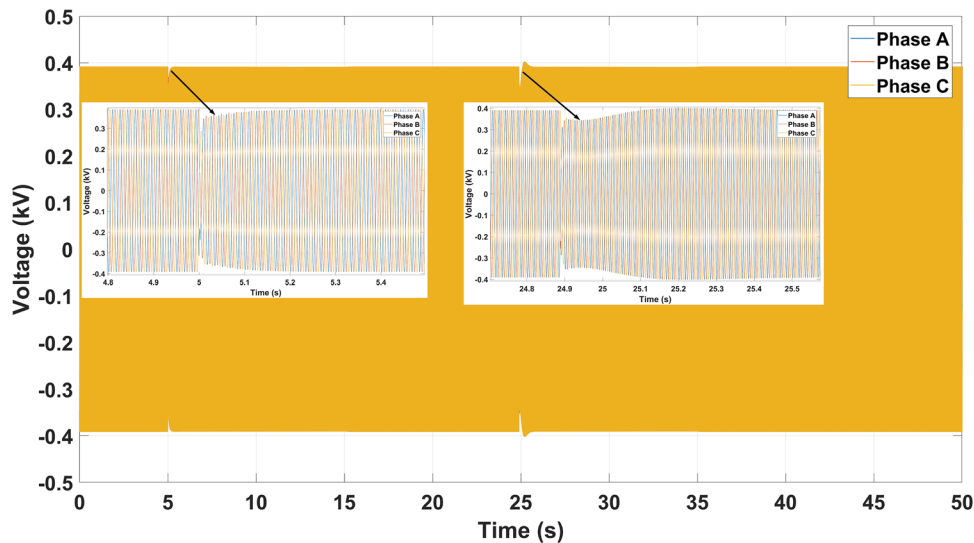


FIGURE 18 LMB three phase AC voltage.

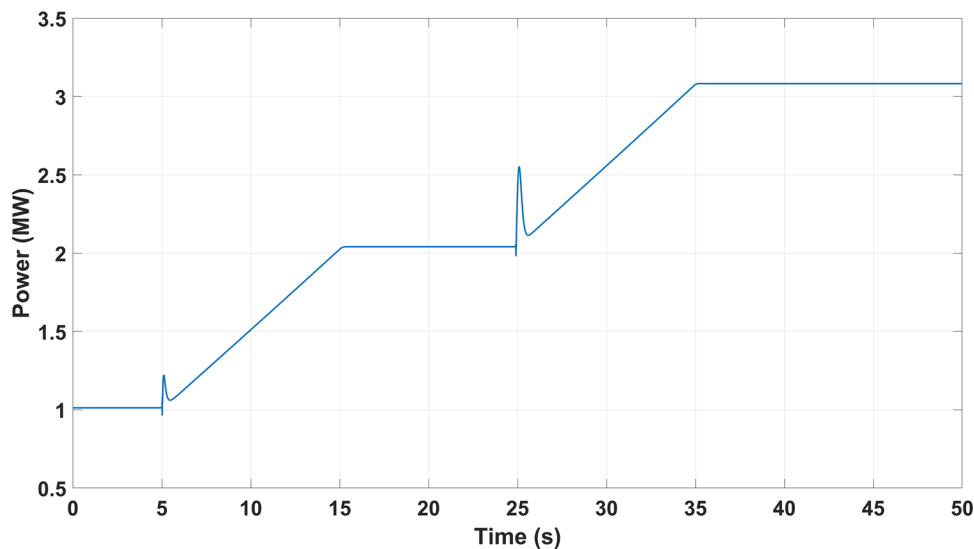


FIGURE 19 Active power dispatch by the LMB.

59.78 Hz while the system steady state frequency rose to 59.88 Hz. The fast dynamic response of the inverter-based LMB is able to reduce the rate of frequency deviation (from its nominal value to its minimum value) from approximately 0.071 Hz/s with the NRS acting alone to 0.064 Hz/s when coupled with the LMB. The LMB DC current and voltage is as shown in Figure 13.

The LMB DC voltage decreases by approximately 12% at its maximum power dispatch of 3.37 MW. The power dispatch by the LMB based on the power command obtained from the frequency-power droop curve is as shown in Figure 14.

The plot (in Figure 14) also shows the effectiveness of active power controller used in the simulation because it is able to track the power reference (based on the frequency–Watt droop

curve) and dispatch the right amount of power in response to the generators' frequency deviation.

## 5.2 | Grid forming and black start analysis

The ability of the NRS to come online with sole support from the LMB (no grid power) is investigated in this subsection. The schematic for validating the black start capability of the NRS-LMB is shown in Figure 15

In this scenario, the LMB provides the NRS with power to energize its auxiliary loads, which are required to bring the NRS back online. The auxiliary loads include feedwater pumps, coolant pumps, motors, electrical supplies, protection systems etc. The black start scenario is simulated by assuming a base

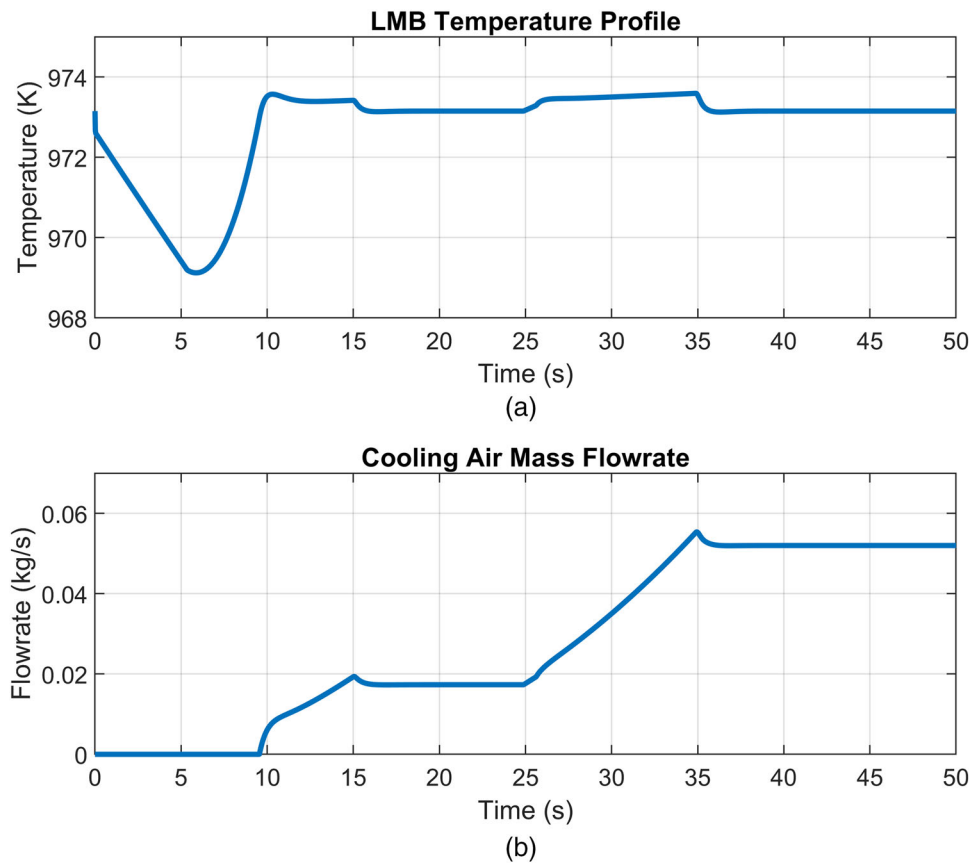


**FIGURE 20** LMB temperature and cooling air mass flow rate profiles during discharging.

load of 1 MW that must be powered by the LMB immediately upon a loss of grid power, aggregated pump loads of 1 MW that ramp up by 100 kW/s for 10 s, and additional aggregated pump loads of 1 MW that ramp up by 100 kW/s for the next 10 s.

The results from the described black start scenario is shown in Figures 16–19. Figure 16 shows the dynamic frequency response of the LMB as it powers up the NRS base and aggregated motor loads.

The first 1 MW of aggregated pump loads is brought online after 5 s and ramped up over the next several seconds. The frequency nadir at 5 s is 59.6 Hz while the maximum frequency deviation is 60.18 Hz. The system's frequency reaches a steady state within 0.5 s after the application of the 1 MW motor load. The second motor load is switched on at approximately 25 s. The frequency nadir at this instance is 58.7 Hz while the maximum frequency deviation is 60.7 Hz. The system's frequency also settles back at steady state within 0.5 s. The lower frequency nadir when the second motor load is switched on is due to the increased aggregated loads powered by the LMB and to the existing 1 MW motor already powered on by the LMB.

The AC current delivered by the LMB is as shown in Figure 17. The plot shows the dynamic response of the LMB current as the power demand by the NRS auxiliary load changes with time. The spike in the AC current when each motor load

is turned on is due to the inrush current drawn by the motor during startup. The result shows that the LMB was able to cope with this current demand.

The LMB's three phase AC voltage during the black start process is shown in Figure 18. The figure reveals a slight voltage drop in the phase voltage during the start of the motor loads due to the inrush current. The LMB voltage controller is able to bring the voltage back to its nominal rated value after dynamic transient caused by the motor inrush current.

The total power dispatched to the auxiliary loads during black start is shown in Figure 19. The results further show the dynamic response of the LMB as it powers the base load and the motor loads. The spikes at 5 and 25 s are due to the startup currents drawn by the motor loads.

The temperature control mechanism is tested using the power dispatch profile as an input to the thermal LMB model. This is to ensure that the LMB remains within its nominal operating temperature during its entire dynamic operation. The energy block's temperature and its corresponding cooling air flow rate are shown in Figure 20. The results show that the cooling air effectively keeps the LMB's temperature within its nominal value during the black start period despite the significant change in power demand from the LMB with increase in the startup loads.



## 6 | CONCLUSIONS AND FUTURE WORK

This paper presented the modelling and performance analysis of a coupled LMB with an NRS. This coupling is done to improve the dynamic response of the NRS and its ability to provide black start capability when grid power is unavailable. The NRS (which consists of the HTGR and sCO<sub>2</sub>) is modelled in Dymola, while the LMB is modelled in RTDS-RSCAD. The simulation data between both platforms were shared using the TCP/IP communication protocol. The models developed in this work are based on electrochemical and thermal physics that govern the dynamic response of the integrated system so that the models are realistic and scalable for future commercial megawatt applications. We investigated the dynamic performance of the NRS-LMB integration by testing it on the IEEE 9 bus system. Including LMB with an NRS improved fast voltage and frequency regulation in both grid-forming and grid-following operational modes. Simulations of a 20 MW NRS coupled in a grid environment near a 10 MW load that suddenly increased to 20 MW caused a maximum frequency nadir of 59.68 Hz. Including a 20 MW LMB in the simulation decreased the frequency nadir to 59.78 Hz. This research aligns with the nuclear industry's growing interest in pairing reactors with energy storage. These integrated systems offer significant advantages for the grid wherein they can adjust power output (ramping up or down) to meet fluctuating grid demands, provide dispatchable power by generating electricity for specific times, and crucially, support net-zero clean energy goals by producing zero carbon emissions from both the reactor as well as the energy storage system. In addition, such integrated systems would increase grid reliability and stability, and allow for increased penetration of renewable energy.

For future work, a techno-economic analysis of the proposed integrated system is being carried out to understand the levelized costs of the system. This will include the levelized costs of storage as well as electricity and will utilize Idaho National Laboratory's Holistic Energy Resource Optimization Network (HERON) software framework to determine if the proposed design is viable in a given market, and how to optimize the design using regression analysis.

## AUTHOR CONTRIBUTIONS

**Amey Shigrekar:** Model development; simulation; writing. **Jiangkai Peng:** Model development; simulation; writing. **Temitayo O. Olowu:** Model development; simulation; writing. **Fernando Gallego Dias:** Model development; supervision. **Tyler Westover:** Project PI; supervision; review and editing.

## ACKNOWLEDGMENTS

This paper and the work described were supported through the INL Laboratory Directed Research and Development (LDRD) Program under DOE Idaho Operations Office Contract DE-AC07-05ID14517.

## CONFLICT OF INTEREST STATEMENT

The authors declare no conflicts of interest.

## DATA AVAILABILITY STATEMENT

Research data are not shared.

## ORCID

Temitayo O. Olowu  <https://orcid.org/0000-0002-1412-3138>

## REFERENCES

- Nalley, S., LaRose, A.: Annual energy outlook 2022 (AEO2022). Energy Information Agency. 2022 Mar 3;23.
- Mohanpurkar, M., Luo, Y., Terlip, D., Dias, F., Harrison, K., Eichman, J., Hovsapian, R., Kurtz, J.: Electrolyzers enhancing flexibility in electric grids. *Energies* 10(11), (2017). <https://doi.org/10.3390/en10111836>
- Shahbazbegian, V., Shafie-khah, M., Laaksonen, H., Strbac, G., Ameli, H.: Resilience-oriented operation of microgrids in the presence of power-to-hydrogen systems. *Appl. Energy* 348, 121429 (2023). <https://doi.org/10.1016/j.apenergy.2023.121429>
- What is generation capacity? <https://www.energy.gov/ne/articles/what-generation-capacity> (2020).
- Bragg-Sitton, S.M., Boardman, R., Rabiti, C., O'Brien, J.: Reimagining future energy systems: overview of the US program to maximize energy utilization via integrated nuclear-renewable energy systems. *Int. J. Energy Res.* 44(10), 8156–8169 (2020)
- Saeed, R.M., Shigrek, A., Mikkelsen, D.M., George Rigby, A.C., Yang Hui Otani, C.M., Garrouste, M., Frick, K.L., Bragg-Sitton, S.M.: Multilevel Analysis, Design, and Modeling of Coupling Advanced Nuclear Reactors and Thermal Energy Storage in an Integrated Energy System. Idaho National Laboratory, Idaho Falls, ID (2022)
- Kiomarsi, F., Shojaei, A.A., Soltani, S.: Choosing an optimal connecting place of a nuclear power plant to a power system using Monte Carlo and LHS methods. *Nucl. Eng. Technol.* 52(7), 1587–1596 (2020). <https://doi.org/10.1016/j.net.2020.01.003>
- Kiomarsi, F., Shojaei, A.A., Soltani, S., Lotfi, H.: Presenting new approach for optimal placement of nuclear power plant connected to the grid after the trip. *SN Appl. Sci.* 3, 1–14 (2021)
- Breeze, P.: Power Generation Technologies. Newnes, London (2019)
- Nurfahana, A.J., Izhar, A.H., Ridzuan, A.M.: The preliminary study of high temperature gas cooled reactors (HTGRs) technology. Paper presented at the 2015 nuclear technical convention, Malaysian Nuclear Agency, Kajang, 3–5 November 2015
- Shelton, W., Weiland, N., Shultz, T., White, C.W.: Supercritical Carbon Dioxide (sCO<sub>2</sub>) Cycle as an Efficiency Improvement Opportunity for Air-Fired Coal Combustion. National Energy Technology Laboratory, Pittsburgh, PA (2019)
- Dawson, L.A., Cook, M.A.: Integrated Cyber/Physical Impact Analysis to Secure US Critical Infrastructure. Sandia National Laboratory, Albuquerque, NM (2016)
- Agarwal, D., Potnuru, R., Kaushik, C., Darla, V.R., Kulkarni, K., Garg, A., Gupta, R.K., Tiwari, N., Nalwa, K.S.: Recent advances in the modeling of fundamental processes in liquid metal batteries. *Renewable Sustainable Energy Rev.* 158, 112167 (2022)
- Ning, X., Phadke, S., Chung, B., Yin, H., Burke, P., Sadoway, D.R.: Self-healing Li–Bi liquid metal battery for grid-scale energy storage. *J. Power Sources* 275, 370–376 (2015)
- Wang, K., Jiang, K., Chung, B., Ouchi, T., Burke, P.J., Boysen, D.A., Bradwell, D.J., Kim, H., Muecke, U., Sadoway, D.R.: Lithium–antimony–lead liquid metal battery for grid-level energy storage. *Nature* 514, 348–350 (2014)
- Bradwell, D.J., Kim, H., Sirk, A.H., Sadoway, D.R.: Magnesium–antimony liquid metal battery for stationary energy storage. *J. Am. Chem. Soc.* 134(4), 1895–1897 (2012)
- Kim, H., Boysen, D.A., Ouchi, T., Sadoway, D.R.: Calcium–bismuth electrodes for large-scale energy storage (liquid metal batteries). *J. Power Sources* 241, 239–248 (2013)
- Ambri: Ambri batteries for clean energy. <https://ambri.com/benefits/> [Accessed 11-12-2022].

19. Yin, H., Chung, B., Chen, F., Ouchi, T., Zhao, J., Tanaka, N., Sadoway, D.R.: Faradaically selective membrane for liquid metal displacement batteries. *Nat. Energy* 3(2), 127–131 (2018)
20. Kim, H., Boysen, D.A., Newhouse, J.M., Spatocco, B.L., Chung, B., Burke, P.J., Bradwell, D.J., Jiang, K., Tomaszowska, A.A., Wang, K., et al.: Liquid metal batteries: past, present, and future. *Chem. Rev.* 113(3), 2075–2099 (2013)
21. Kendall, J.: Gas Turbine Power Conversion Systems for Modular HGTRs. International Atomic Energy Agency, Vienna (2001)
22. Harvego, E.A., McKellar, M.G.: Evaluation and Optimization of a Supercritical Carbon Dioxide Power Conversion Cycle for Nuclear Applications. Idaho National Laboratory, Idaho Falls, ID (2011)
23. DYMOLA: DYMOLA systems engineering multi-engineering modeling and simulation based on Modelica and FMI. <https://www.3ds.com/products-services/catia/products/dymola/> [Accessed 01-12-2022].
24. RTDS: RSCAD FX: Real-time simulation software package. <https://knowledge.rtds.com/hc/en-us/articles/360046352893-RSCAD-FX-Real-Time-Simulation-Software-Package> [Accessed 01-12-2022].
25. HYBRID. <https://github.com/idaholab/HYBRID> (2022), [Accessed 20-12-2022].
26. Bell, I.H., Wronski, J., Quoilin, S., Lemort, V.: Pure and pseudo-pure fluid thermophysical property evaluation and the open-source thermophysical property library coolprop. *Ind. Eng. Chem. Res.* 53(6), 2498–2508 (2014)
27. Mikkelsen, D.M., Shigrek, A., Hancock, S.G., Frick, K.L., Epiney, A.S.: Delivery of Dynamic Thermal Energy Storage Models and Advanced Reactor Concept Models to the Hybrid Repository. Idaho National Laboratory, Idaho Falls, ID (2022)
28. Newhouse, J.M.: Modeling the operating voltage of liquid metal battery cells. Ph.D. Thesis, Massachusetts Institute of Technology (2014)
29. Shen, Y., Zikanov, O.: Thermal convection in a liquid metal battery. *Theor. Comput. Fluid Dyn.* 30(4), 275–294 (2016)

**How to cite this article:** Shigrek, A., Peng, J., Olowu, T.O., Gallego Dias, F., Westover, T.: Modelling and analysis of nuclear reactor system coupled with a liquid metal battery. *J. Eng.* 2024, e12382 (2024). <https://doi.org/10.1049/tje2.12382>